

Searches for Extended and Point-like Neutrino Sources with Four Years of IceCube Data

IceCube Collaboration: M. G. Aartsen¹, M. Ackermann², J. Adams³, J. A. Aguilar⁴, M. Ahlers⁵, M. Ahrens⁶, D. Altmann⁷, T. Anderson⁸, C. Argüelles⁵, T. C. Arlen⁸, J. Auffenberg⁹, X. Bai¹⁰, S. W. Barwick¹¹, V. Baum¹², J. J. Beatty^{13,14}, J. Becker Tjus¹⁵, K.-H. Becker¹⁶, S. BenZvi⁵, P. Berghaus², D. Berley¹⁷, E. Bernardini², A. Bernhard¹⁸, D. Z. Besson¹⁹, G. Binder^{20,21}, D. Bindig¹⁶, M. Bissok⁹, E. Blaufuss¹⁷, J. Blumenthal⁹, D. J. Boersma²², C. Boehm⁶, F. Bos¹⁵, D. Bose²³, S. Böser²⁴, O. Botner²², L. Brayeur²⁵, H.-P. Bretz², A. M. Brown³, J. Casey²⁶, M. Casier²⁵, E. Cheung¹⁷, D. Chirkin⁵, A. Christov⁴, B. Christy¹⁷, K. Clark²⁷, L. Classen⁷, F. Clevermann²⁸, S. Coenders¹⁸, D. F. Cowen^{8,29}, A. H. Cruz Silva², M. Danninger⁶, J. Daughhetee²⁶, J. C. Davis¹³, M. Day⁵, J. P. A. M. de André⁸, C. De Clercq²⁵, S. De Ridder³⁰, P. Desiati⁵, K. D. de Vries²⁵, M. de With³¹, T. DeYoung⁸, J. C. Díaz-Vélez⁵, M. Dunkman⁸, R. Eagan⁸, B. Eberhardt¹², B. Eichmann¹⁵, J. Eisch⁵, S. Euler²², P. A. Evenson³², O. Fadiran⁵, A. R. Fazely³³, A. Fedynitch¹⁵, J. Feintzeig⁵, J. Felde¹⁷, T. Feusels³⁰, K. Filimonov²¹, C. Finley⁶, T. Fischer-Wasels¹⁶, S. Flis⁶, A. Franckowiak²⁴, K. Frantzen²⁸, T. Fuchs²⁸, T. K. Gaisser³², J. Gallagher³⁴, L. Gerhardt^{20,21}, D. Gier⁹, L. Gladstone⁵, T. Glüsenskamp², A. Goldschmidt²⁰, G. Golup²⁵, J. G. Gonzalez³², J. A. Goodman¹⁷, D. Góra², D. T. Grandmont³⁵, D. Grant³⁵, P. Gretskov⁹, J. C. Groh⁸, A. Groß¹⁸, C. Ha^{20,21}, C. Haack⁹, A. Haj Ismail³⁰, P. Hallen⁹, A. Hallgren²², F. Halzen⁵, K. Hanson³⁶, D. Hebecker²⁴, D. Heereman³⁶, D. Heinen⁹, K. Helbing¹⁶, R. Hellauer¹⁷, D. Hellwig⁹, S. Hickford³, G. C. Hill¹, K. D. Hoffman¹⁷, R. Hoffmann¹⁶, A. Homeier²⁴, K. Hoshina^{5,37}, F. Huang⁸, W. Huelsnitz¹⁷, P. O. Hulth⁶, K. Hultqvist⁶, S. Hussain³², A. Ishihara³⁸, E. Jacobi², J. Jacobsen⁵, K. Jagielski⁹, G. S. Japaridze³⁹, K. Jero⁵, O. Jlelati³⁰, M. Jurkovic¹⁸, B. Kaminsky², A. Kappes⁷, T. Karg², A. Karle⁵, M. Kauer⁵, J. L. Kelley⁵, A. Kheirandish⁵, J. Kiryluk⁴⁰, J. Kläs¹⁶, S. R. Klein^{20,21}, J.-H. Köhne²⁸, G. Kohlen⁴¹, H. Kolanoski³¹, A. Koob⁹, L. Köpke¹², C. Kopper⁵, S. Kopper¹⁶, D. J. Koskinen⁴², M. Kowalski²⁴, A. Kriesten⁹, K. Krings⁹, G. Kroll¹², M. Kroll¹⁵, J. Kunnen²⁵, N. Kurahashi⁵, T. Kuwabara³², M. Labare³⁰, D. T. Larsen⁵, M. J. Larson⁴², M. Lesiak-Bzdak⁴⁰, M. Leuermann⁹, J. Leute¹⁸, J. Lünemann¹², O. Macías³, J. Madsen⁴³, G. Maggi²⁵, R. Maruyama⁵, K. Mase³⁸, H. S. Matis²⁰, R. Maunu¹⁷, F. McNally⁵, K. Meagher¹⁷, M. Medici⁴², A. Meli³⁰, T. Meures³⁶, S. Miarecki^{20,21}, E. Middell², E. Middlemas⁵, N. Milke²⁸, J. Miller²⁵, L. Mohrmann², T. Montaruli⁴, R. Morse⁵, R. Nahnauer², U. Naumann¹⁶, H. Niederhausen⁴⁰, S. C. Nowicki³⁵, D. R. Nygren²⁰, A. Obertacke¹⁶, S. Odrowski³⁵, A. Olivas¹⁷, A. Omairat¹⁶, A. O'Murchadha³⁶, T. Palczewski⁴⁴, L. Paul⁹, Ö. Penek⁹, J. A. Pepper⁴⁴, C. Pérez de los Heros²², C. Pfendner¹³, D. Pieloth²⁸, E. Pinat³⁶, J. Posselt¹⁶, P. B. Price²¹, G. T. Przybylski²⁰, J. Pütz⁹, M. Quinnan⁸, L. Rädcl⁹, M. Rameez⁴, K. Rawlins⁴⁵, P. Redl¹⁷, I. Rees⁵, R. Reimann⁹, E. Resconi¹⁸, W. Rhode²⁸, M. Richman¹⁷, B. Riedel⁵, S. Robertson¹, J. P. Rodrigues⁵, M. Rongen⁹, C. Rott²³, T. Ruhe²⁸, B. Ruzybayev³², D. Ryckbosch³⁰, S. M. Saba¹⁵, H.-G. Sander¹², J. Sandroos⁴², M. Santander⁵, S. Sarkar^{42,46}, K. Schatto¹², F. Scheriau²⁸, T. Schmidt¹⁷, M. Schmitz²⁸, S. Schoenen⁹, S. Schöneberg¹⁵, A. Schönwald², A. Schukraft⁹, L. Schulte²⁴, O. Schulz¹⁸, D. Seckel³², Y. Sestayo¹⁸, S. Seunarine⁴³, R. Shanidze², C. Sheremata³⁵, M. W. E. Smith⁸,

D. Soldin¹⁶, G. M. Spiczak⁴³, C. Spiering², M. Stamatikos^{13,47}, T. Stanev³², N. A. Stanisha⁸,
A. Stasik²⁴, T. Stezelberger²⁰, R. G. Stokstad²⁰, A. Stöbl², E. A. Strahler²⁵, R. Ström²²,
N. L. Strotjohann²⁴, G. W. Sullivan¹⁷, H. Taavola²², I. Taboada²⁶, A. Tamburro³², A. Tepe¹⁶,
S. Ter-Antonyan³³, A. Terliuk², G. Tešić⁸, S. Tilav³², P. A. Toale⁴⁴, M. N. Tobin⁵, D. Tosi⁵,
M. Tselengidou⁷, E. Unger¹⁵, M. Usner²⁴, S. Vallecorsa⁴, N. van Eijndhoven²⁵,
J. Vandenbroucke⁵, J. van Santen⁵, M. Vehring⁹, M. Voge²⁴, M. Vraeghe³⁰, C. Walck⁶,
M. Wallraff⁹, Ch. Weaver⁵, M. Wellons⁵, C. Wendt⁵, S. Westerhoff⁵, B. J. Whelan¹,
N. Whitehorn⁵, C. Wichary⁹, K. Wiebe¹², C. H. Wiebusch⁹, D. R. Williams⁴⁴, H. Wissing¹⁷,
M. Wolf⁶, T. R. Wood³⁵, K. Woschnagg²¹, D. L. Xu⁴⁴, X. W. Xu³³, J. P. Yanez², G. Yodh¹¹,
S. Yoshida³⁸, P. Zarzhitsky⁴⁴, J. Ziemann²⁸, S. Zierke⁹, and M. Zoll⁶

-
- ¹School of Chemistry & Physics, University of Adelaide, Adelaide SA, 5005 Australia
- ²DESY, D-15735 Zeuthen, Germany
- ³Dept. of Physics and Astronomy, University of Canterbury, Private Bag 4800, Christchurch, New Zealand
- ⁴Département de physique nucléaire et corpusculaire, Université de Genève, CH-1211 Genève, Switzerland
- ⁵Dept. of Physics and Wisconsin IceCube Particle Astrophysics Center, University of Wisconsin, Madison, WI 53706, USA
- ⁶Oskar Klein Centre and Dept. of Physics, Stockholm University, SE-10691 Stockholm, Sweden
- ⁷Erlangen Centre for Astroparticle Physics, Friedrich-Alexander-Universität Erlangen-Nürnberg, D-91058 Erlangen, Germany
- ⁸Dept. of Physics, Pennsylvania State University, University Park, PA 16802, USA
- ⁹III. Physikalisches Institut, RWTH Aachen University, D-52056 Aachen, Germany
- ¹⁰Physics Department, South Dakota School of Mines and Technology, Rapid City, SD 57701, USA
- ¹¹Dept. of Physics and Astronomy, University of California, Irvine, CA 92697, USA
- ¹²Institute of Physics, University of Mainz, Staudinger Weg 7, D-55099 Mainz, Germany
- ¹³Dept. of Physics and Center for Cosmology and Astro-Particle Physics, Ohio State University, Columbus, OH 43210, USA
- ¹⁴Dept. of Astronomy, Ohio State University, Columbus, OH 43210, USA
- ¹⁵Fakultät für Physik & Astronomie, Ruhr-Universität Bochum, D-44780 Bochum, Germany
- ¹⁶Dept. of Physics, University of Wuppertal, D-42119 Wuppertal, Germany
- ¹⁷Dept. of Physics, University of Maryland, College Park, MD 20742, USA
- ¹⁸Technische Universität München, D-85748 Garching, Germany
- ¹⁹Dept. of Physics and Astronomy, University of Kansas, Lawrence, KS 66045, USA
- ²⁰Lawrence Berkeley National Laboratory, Berkeley, CA 94720, USA
- ²¹Dept. of Physics, University of California, Berkeley, CA 94720, USA
- ²²Dept. of Physics and Astronomy, Uppsala University, Box 516, S-75120 Uppsala, Sweden
- ²³Dept. of Physics, Sungkyunkwan University, Suwon 440-746, Korea
- ²⁴Physikalisches Institut, Universität Bonn, Nussallee 12, D-53115 Bonn, Germany
- ²⁵Vrije Universiteit Brussel, Dienst ELEM, B-1050 Brussels, Belgium
- ²⁶School of Physics and Center for Relativistic Astrophysics, Georgia Institute of Technology, Atlanta, GA 30332, USA
- ²⁷Dept. of Physics, University of Toronto, Toronto, Ontario, Canada, M5S 1A7
- ²⁸Dept. of Physics, TU Dortmund University, D-44221 Dortmund, Germany
- ²⁹Dept. of Astronomy and Astrophysics, Pennsylvania State University, University Park, PA 16802, USA
- ³⁰Dept. of Physics and Astronomy, University of Gent, B-9000 Gent, Belgium

ABSTRACT

We present results on searches for point-like sources of neutrinos using four years of IceCube data, including the first year of data from the completed 86-string detector. The total livetime of the combined dataset is 1,373 days. For an E^{-2} spectrum the median sensitivity at 90% C.L. is $\sim 10^{-12} \text{ TeV}^{-1} \text{ cm}^{-2} \text{ s}^{-1}$ for energies between 1 TeV–1 PeV in the northern sky and $\sim 10^{-11} \text{ TeV}^{-1} \text{ cm}^{-2} \text{ s}^{-1}$ for energies between 100 TeV – 100 PeV in the southern sky. The sensitivity has improved from both the additional year of data and the introduction of improved reconstructions compared to previous publications. In addition, we present the first results from an all-sky search for extended sources of neutrinos. We update results of searches for neutrino emission from stacked catalogs of sources, and test five new catalogs; two of Galactic supernova remnants and three of active galactic nuclei. In all cases, the data are compatible with the background-only hypothesis, and upper limits on the flux of muon neutrinos are reported for the sources considered.

Subject headings: cosmic neutrinos, neutrino sources, neutrino telescopes, Cherenkov light detection

³¹Institut für Physik, Humboldt-Universität zu Berlin, D-12489 Berlin, Germany

³²Bartol Research Institute and Dept. of Physics and Astronomy, University of Delaware, Newark, DE 19716, USA

³³Dept. of Physics, Southern University, Baton Rouge, LA 70813, USA

³⁴Dept. of Astronomy, University of Wisconsin, Madison, WI 53706, USA

³⁵Dept. of Physics, University of Alberta, Edmonton, Alberta, Canada T6G 2E1

³⁶Université Libre de Bruxelles, Science Faculty CP230, B-1050 Brussels, Belgium

³⁷Earthquake Research Institute, University of Tokyo, Bunkyo, Tokyo 113-0032, Japan

³⁸Dept. of Physics, Chiba University, Chiba 263-8522, Japan

³⁹CTSPS, Clark-Atlanta University, Atlanta, GA 30314, USA

⁴⁰Dept. of Physics and Astronomy, Stony Brook University, Stony Brook, NY 11794-3800, USA

⁴¹Université de Mons, 7000 Mons, Belgium

⁴²Niels Bohr Institute, University of Copenhagen, DK-2100 Copenhagen, Denmark

⁴³Dept. of Physics, University of Wisconsin, River Falls, WI 54022, USA

⁴⁴Dept. of Physics and Astronomy, University of Alabama, Tuscaloosa, AL 35487, USA

⁴⁵Dept. of Physics and Astronomy, University of Alaska Anchorage, 3211 Providence Dr., Anchorage, AK 99508, USA

⁴⁶Dept. of Physics, University of Oxford, 1 Keble Road, Oxford OX1 3NP, UK

⁴⁷NASA Goddard Space Flight Center, Greenbelt, MD 20771, USA

1. Introduction

Neutrinos have unique properties that can be used to probe diverse astrophysical processes. Produced in interactions of protons and nuclei with ambient radiation and matter, their low cross-section allows them to travel astronomical distances without experiencing significant absorption. Unlike charged cosmic rays which change direction as they pass through galactic and intergalactic magnetic fields, neutrinos preserve their directional information as they travel straight from the source to Earth. Astrophysical neutrinos are also tracers of hadronic interactions, and the identification of these neutrino sources may help to clarify cosmic ray acceleration processes (Anchordoqui & Montaruli 2010; Anchordoqui *et al.* 2014; Becker 2008; Halzen & Hooper 2002; Learned & Mannheim 2000). Candidate sources for cosmic ray acceleration (and therefore neutrino emission) include Supernova Remnant (SNR) shocks (Alvarez-Muñiz & Halzen 2002; Cavasinni *et al.* 2006; Gonzalez-Garcia *et al.* 2014; De Marco *et al.* 2006; Vissani *et al.* 2011), Active Galactic Nuclei (AGN) jets (Essey *et al.* 2010; Kalashev *et al.* 2013; Murase *et al.* 2014; Sironi & Spitkovsky 2011; Stecker *et al.* 1991; Waxman & Bahcall 1999), Starburst Galaxies (Lacki *et al.* 2011; Loeb & Waxman 2006; Murase *et al.* 2013; Romero & Torres 2003), and Gamma-Ray Bursts (GRBs) (Guetta *et al.* 2004; Mészáros 2006; Waxman & Bahcall 1997).

IceCube recently found evidence for a diffuse flux of high-energy astrophysical neutrinos (Aartsen *et al.* 2013d, 2014b), observing a 5.7σ excess of events between ~ 50 TeV and 2 PeV deposited within the detector. The 37 observed events are consistent with an $E^{-2.3}$ neutrino flux at the level of $1.5 \times 10^{-11} \text{ TeV}^{-1} \text{ cm}^{-2} \text{ s}^{-1} \text{ sr}^{-1}$ (normalized at 100 TeV), with a neutrino flavor ratio of 1:1:1. While these events have established unequivocally that astrophysical neutrinos exist, their sources have not yet been identified. One challenge is that only $\sim 20\%$ of the events in that sample are associated with a high-energy muon which leaves a visible track in the detector. The remaining events without a track have a poor angular resolution of $\sim 15^\circ$.

This paper presents the latest results of searches for point sources of astrophysical neutrinos with a sample of track-like events associated with ν_μ (and some ν_τ) charged current interactions observed by the IceCube Neutrino Observatory. These events have an excellent angular resolution of $\leq 1^\circ$ and hence allow us to point back towards the source. As the main signature we focus on is the resultant muon, the interaction vertex is not required to lie inside the detector as in Ref. (Aartsen *et al.* 2013d, 2014b) and the effective volume is hence effectively enhanced. The results of an all-sky search, a search among a catalog of candidate neutrino emitters and stacked source catalog searches with a similar sample of events from the data collected between 2008-2011 are published in Ref. (Aartsen *et al.* 2013c). Here we update these analyses by adding the first year of data from the complete 86-string detector configuration, collected between May 2011 - May 2012. Five new stacking analyses based on newly available catalogs are also presented here.

In this paper we describe the results of the first all-sky survey by IceCube looking for extended regions of neutrino emission. H.E.S.S. has surveyed the Galactic Plane looking for γ -ray emissions above 200 GeV, revealing previously unknown extended regions emitting to TeV energies (Carrigan

et al. 2013). The Fermi/LAT survey above 100 GeV also shows the same bright extended sources. These extended regions may be unidentified SNRs associated with molecular clouds, which are also expected to be spatially extended sources of neutrinos (Gonzalez-Garcia *et al.* 2014; Mandelartz & Tjus 2013). Outside the Galaxy, large clusters of galaxies such as Virgo are promising neutrino emitters expected to have spatial extensions (De Marco *et al.* 2006; Murase *et al.* 2008; Murase & Beacom 2012; Wolfe *et al.* 2008). It is therefore important not to limit the search for sources of neutrinos uniquely to point-like sources but also to extended regions as shown in Ref. (Tchernin *et al.* 2013).

Section 2 describes the IceCube detector and the event selection for data from the first year of the completed detector. Event selections for data from the previous years of operation of the detector have been extensively described in Ref. (Aartsen *et al.* 2013c) and Ref. (Abbasi *et al.* 2011). The methodology used to combine data from different years and detector configurations and to optimize the searches for various source signal hypotheses is described in Sec. 3. Section 4 presents the results of the analyses, which are discussed within the context of recent models of astrophysical neutrino emission. Conclusions are drawn in Sec. 5.

2. Detector and Event Selection

The IceCube Observatory is a cubic-kilometer-sized Cherenkov detector embedded in the ice at the geographic South Pole (Achterberg *et al.* 2006). Optimized to detect neutrinos above TeV energies, it consists of 5160 photomultiplier tubes (PMTs) instrumented along 86 cables (called strings) at depths of 1450 - 2450 m beneath the surface of the ice sheet. Each PMT is housed in a digital optical module (DOM), consisting of a pressure-resistant sphere with on-board digitization and calibration LEDs (Abbasi *et al.* 2010). The DOMs detect Cherenkov photons emitted by charged leptons that traverse the detector (Abbasi *et al.* 2009). This analysis uses data taken between April 2008 and May 2012. During this period, IceCube ran in four different configurations. Three years of data are from the partial detector composed of 40-, 59-, and 79-strings, respectively, and are fully described in Ref. (Aartsen *et al.* 2013c). The following year of data was taken with the completed 86-string array. The used selection procedure and event reconstructions are similar to those applied to the previous data.

2.1. Data Reduction and Reconstruction for the IC86-1 Data Sample

Data acquisition is triggered by requiring four pairs of neighboring or next-to-neighboring DOMs to observe photoelectrons within a $5 \mu\text{s}$ time window. 2.5 kHz of data satisfy this criterion. A combination of real-time filtering at the South Pole and subsequent offline CPU-intensive processing reduces the data rate to 2 Hz by rejecting mis-reconstructed events. At this stage the data are dominated by atmospheric muons from cosmic rays; both well reconstructed down-going muons

in the southern sky and down-going muons mis-reconstructed as up-going muons in the northern sky. The data is further reduced via quality cuts using simple reconstructions and event quality parameters followed by advanced likelihood-based muon reconstructions. The simple reconstruction removes scattered photon hits before estimating the muon position and direction via a linear fit with reduced weights for outliers (Aartsen *et al.* 2013b). This fit serves as a seed for more advanced likelihood reconstructions, including the multi-photoelectron (MPE) likelihood. This algorithm includes a probabilistic distribution function (PDF) that describes the scattering of photons in the ice, and is fully described in Ref. (Ahrens *et al.* 2004).

In the processing of data from the first year of the full detector, two new muon reconstructions were used to determine event directions and reject background. The first reconstructs the muon direction by applying the MPE likelihood four times. Each iteration uses a bootstrapped pulse series, extracted randomly from the measured pulses. This is done using a multinomial distribution weighted by charge, so that high charge pulses are more likely to be selected than low ones. The results of these four reconstructions are averaged together to seed one reconstruction using the complete pulses. Of these five fit results, the one with the best likelihood value is selected and saved. Compared to the single-iteration MPE fit, this process reduces the rate of downgoing atmospheric muons mis-reconstructed as upgoing muons by 30%, while improving the neutrino median angular resolution from 0.7° to 0.6° at 30 TeV.

This iterative fit also serves as a seed for the second reconstruction algorithm, which provides a more accurate result by modeling the optical properties of the Antarctic ice sheet. While previous reconstructions use analytic approximations to describe the timing distribution of Cherenkov photons arriving at a given PMT (Ahrens *et al.* 2004), here we use a parametrization of a Monte Carlo simulation. Photon transport is simulated using a depth-dependent model of scattering and absorption in the ice (Aartsen *et al.* 2013a). The arrival time of a photon is a function of the orientation and depth of the muon source and the displacement vector between the muon and the receiving PMT. Photons are simulated for different muon-receiver configurations, and a multi-dimensional spline surface is fit to the resulting arrival time distributions (Whitehorn *et al.* 2013). These splines are used as PDFs in the MPE likelihood. Compared to previous IceCube point source analyses (Aartsen *et al.* 2013c), this reconstruction algorithm leads to a 26% improvement in neutrino median angular resolution at 30 TeV (see Fig. 1). As carried out in previous years, the uncertainty in the angular reconstruction for each event is estimated by fitting a paraboloid to the likelihood space around the reconstructed direction, following the method described in (Abbasi *et al.* 2011; Neunh"offer 2006).

After reconstructing the direction of each event, a separate algorithm fits for the muon energy loss along its track. In the fourth year of data, the energy reconstruction uses an analytic approximation to model the muon light yield at the receiving DOMs as a function of the orientation and depth of the muon (Aartsen *et al.* 2014a).

2.2. Selection of the Final Sample

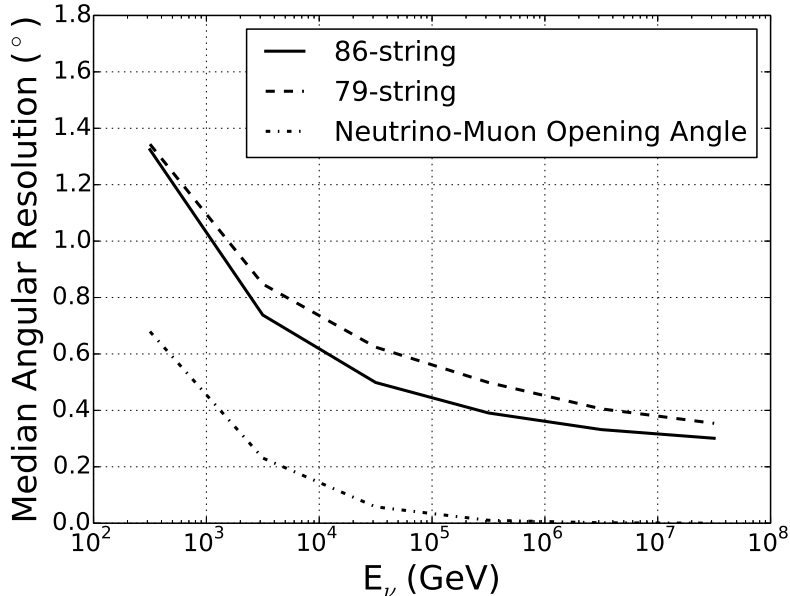


Fig. 1.— Median angular resolution (angle between reconstructed muon track and neutrino direction) as a function of neutrino energy for simulated northern hemisphere event samples from the 86-string (solid) and 79-string (dashed) detector configurations. The improvement is due to the new reconstruction algorithm. At 30 TeV, the 40 and 59 string event selections (not shown) give angular resolutions of $\sim 0.8^\circ$ and $\sim 0.75^\circ$, respectively (Aartsen *et al.* 2013c). The dash-dotted line shows the median kinematic opening angle between the neutrino and muon.

From the 2 Hz of remaining data (still dominated by the atmospheric muon background), 4.8 mHz of events are selected for the final analysis sample. In the northern sky the mis-reconstructed muon background can be mostly eradicated to isolate a nearly pure sample of up-going atmospheric neutrinos. This is done using a classification algorithm, Boosted Decision Trees (BDTs). Similar to previous IceCube point source analyses (Aartsen *et al.* 2013c), we trained four BDTs in two zenith bands to separate astrophysical neutrino signal from the atmospheric muon background. Cuts on the BDT output scores are optimized to achieve the best discovery potential for both E^{-2} and $E^{-2.7}$ signal spectra. This event selection covers the entire Northern Hemisphere and extends 5° above the horizon, where the Earth and glacial ice still provide a shield from the cosmic ray background.

At an angle of more than 5° above the horizon, a pure neutrino sample cannot be isolated from the high-energy atmospheric muon bundles, which are multiple muons from the same air shower that mimic neutrinos. The background can be reduced by introducing quality cuts and using parameters that select neutrinos and reject muon bundles. One BDT is trained for the entire region using data to describe the background and an E^{-2} neutrino simulation for signal. Of the eleven variables used

in training the BDT, three exploit differences between single muons and bundles. These parameters rely on event topology and energy loss information. Large muon bundles consist of many low-energy muons that typically lose energy at a constant rate as they traverse the detector. Photons from these muon bundles are detected within a wider time range. High-energy neutrino-induced muons instead have relatively stochastic energy loss profiles and narrower photon timing distributions. Likelihood ratios are constructed to judge whether a given data event has timing and energy loss properties more consistent with the simulated signal or the estimated background, and are included in the BDT. To obtain the final sample, a cut on the BDT score is varied with zenith to account for the zenith-dependent properties of the background.

The final data sample for the first year of operation of the 86-string detector has 138,322 events, of which approximately half are in the northern hemisphere. The livetime and rates for all four years of detector data are summarized in Table 1. The neutrino effective area for this selection and the central 90% energy region for three signal spectra are shown in Figure 2. The effective area reaches it’s maximum near the horizon. Far below the horizon high-energy neutrinos suffer from absorption in the Earth. Above the horizon the cuts necessary to remove the background remove a significant portion of the lower-energy signal. As a result the analysis is sensitive to the widest neutrino energy range near the horizon, while in the southern hemisphere the sensitivity rapidly deteriorates at lower energies. The discovery potential as a function of energy and declination is shown in Fig. 3. Compared to the 3-year point source analysis (Aartsen *et al.* 2013c), the addition of the first year of data from the completed detector including improved reconstruction and background rejection techniques leads to a 40 – 50% improvement in the discovery potential, with larger gains at energies below 1 PeV in the southern hemisphere.

3. The Likelihood Search Method

Point-like sources of neutrinos in the sky can be identified by searching for clusters of events significantly incompatible with the atmospheric muon and neutrino background. The significance

no. of strings	live-time [days]	atm. ν s	# up-going	# down-going
40	376	40/day	14,121	22,779
59	348	120/day	43,339	64,230
79	316	180/day	50,857	59,009
86	333	210/day	69,227	69,095

Table 1:: Summary for four different IceCube configurations for point source analyses: The expected atmospheric neutrino rate from MC simulation weighted for the model in Ref. (Honda *et al.* 2007) and numbers of up- and down-going events at final selection level. The upgoing data are dominated by atmospheric neutrinos, while data in the downgoing region are dominated by atmospheric muons.

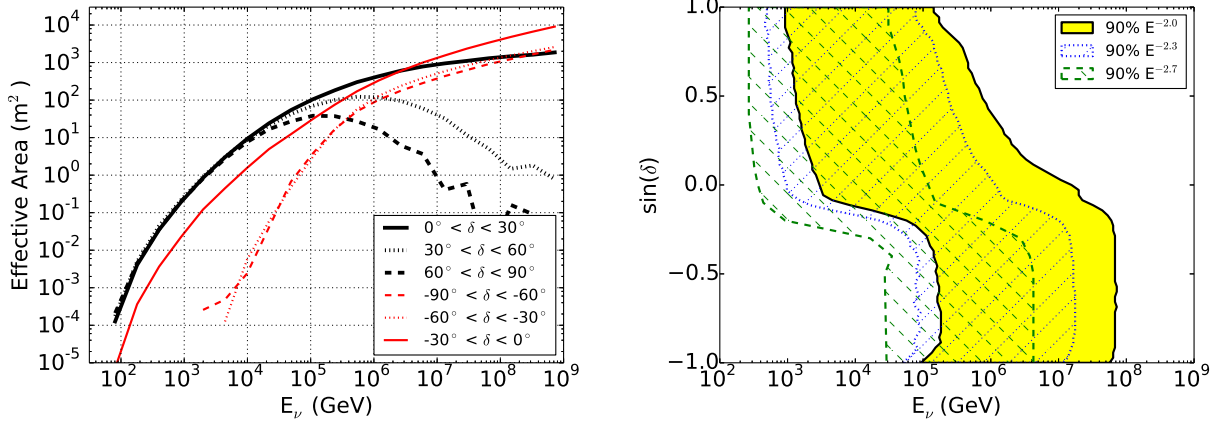


Fig. 2.— Left: Neutrino effective area for the 86-string detector as a function of primary neutrino energy for six declination bands. The effective area is the average of the area for ν_μ and $\bar{\nu}_\mu$. Right: Central 90% energy region for simulated neutrino events as a function of declination. This defines the region where the upper limits for E^{-2} , $E^{-2.3}$, and $E^{-2.7}$ source spectra are valid.

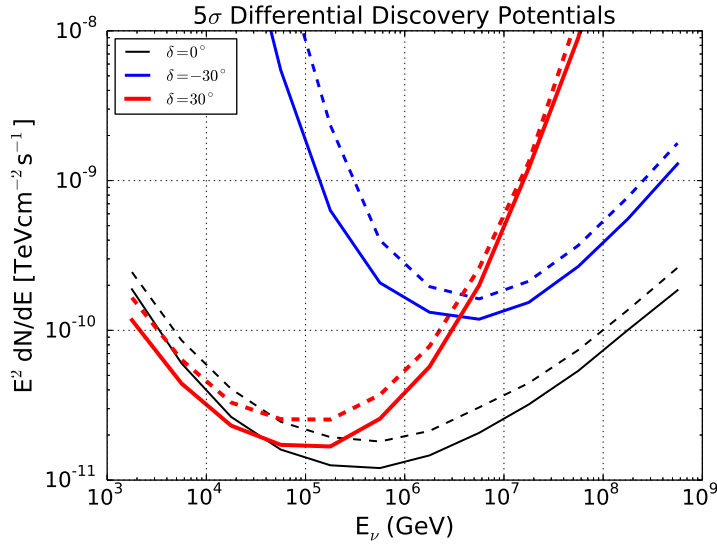


Fig. 3.— Discovery flux as a function of the neutrino energy at 5σ confidence level, for three different declinations (solid lines). Point sources with an E^{-2} spectrum are simulated over a half-decade in energy, and the flux in each bin required for discovery forms the curve above. Results from the previous analysis with 3 years of the data are shown with dashed lines.

is estimated by using an unbinned maximum likelihood ratio test as described in Ref. (Braun *et al.* 2010). The method is expanded to allow for the combination of data from different detector geometries as described in Ref. (Aartsen *et al.* 2013c). In addition to spatial clustering, this method also uses the energies of the events to identify signal events which are expected to have a harder spectrum than that of atmospheric neutrinos and muons. The energy response expected from a neutrino signal from a point source in the sky is modeled using simulation. Since the final event selections are still background dominated, the background estimate is done using real data.

In time integrated searches for a point-like source, the signal PDF \mathcal{S}_i^j for event i observed in detector geometry j is given by:

$$\mathcal{S}_i^j = S_i^j(|\vec{x}_i - \vec{x}_s|, \sigma_i) \mathcal{E}_i^j(E_i, \delta_i, \gamma) \quad (1)$$

Here, the spatial contribution to the PDF is given by S_i^j , which depends on the angular uncertainty of the event σ_i , and the angular difference between the reconstructed direction of the event and the direction of the source. This probability is modeled as a 2-dimensional Gaussian:

$$S_i^j = \frac{1}{2\pi\sigma_i^2} e^{-\frac{|\vec{x}_i - \vec{x}_s|^2}{2\sigma_i^2}}. \quad (2)$$

The contribution from energy $\mathcal{E}_i^j(E_i, \delta_i, \gamma)$ is described in Ref. (Braun *et al.* 2010).

When searching for spatially extended sources the value of σ_i is replaced with $\sigma_i^{\text{eff}} = \sqrt{\sigma_i^2 + \sigma_{\text{src}}^2}$ where σ_{src} is the width of the source. Fig. 4 shows the flux needed for a 5σ discovery for a source located at a given declination as a function of the source extension. The results for two different signal hypotheses are shown; in one the source is always assumed to have no extension while in the other the correct source extension is included in the likelihood description. Naturally, for sources that are truly extended the extended hypothesis is more powerful than the point source assumption. As the real extension of the source increases, the analysis method which assumes that the source is point-like performs worse than the one that takes the extension of the source into account.

To further enhance discovery potentials and sensitivity, stacked searches can be carried out for specific catalogs of similar candidate neutrino sources.

The following is a description of all the searches performed with the four years of IceCube data (similar to those performed in Ref. (Aartsen *et al.* 2013c)):

3.1. All-Sky Searches

These searches are carried out to look for evidence of a source anywhere in the sky and are not motivated by any prior information regarding the position of the sources. The likelihood is

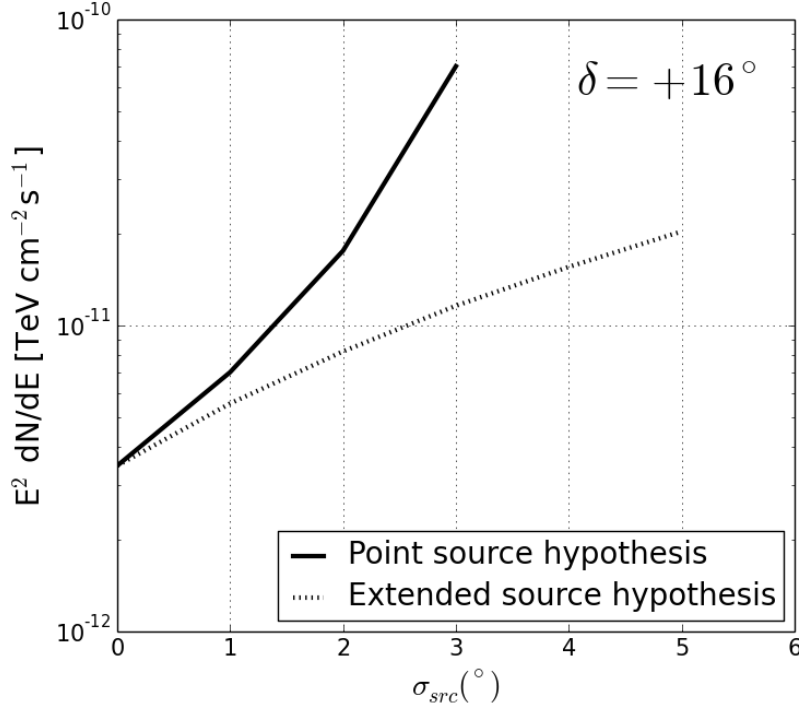


Fig. 4.— Flux needed for a 5σ discovery from a hypothetical source at $\delta = 16^\circ$ as a function of the source extension for the point source signal hypothesis (solid line) and the extended signal hypothesis with the correct extension (dotted line).

evaluated in each direction in the sky. In these searches the number of effective trials is very high and is related to the angular resolution of the telescope and the source extension hypotheses. In order to correct for the trial factor, the same experiment is repeated on an ensemble of scrambled data and the probability of observing a more significant spot than the one observed is obtained.

All Sky Point Source Scan The all-sky scan for point sources of neutrinos that has previously been carried out on data from the incomplete detector configurations is updated to include the first year of data from the complete 86 string detector. In this search the likelihood is evaluated in steps of $0.1^\circ \times 0.1^\circ$ within the declination range -85° to $+85^\circ$ beyond which the scrambling technique is no longer effective.

All Sky Extended Source Scans The search for extended sources is performed in a similar fashion to the all-sky point source searches. In this case the sky is divided into a grid of $0.5^\circ \times 0.5^\circ$ in a similar declination range. For this search a source extension needs to be assumed for the signal. We carry out five different all-sky scans assuming extensions in step

of one degree, from 1° to 5° . An additional trial factor needs to be considered from the additional number of sky scans, however this factor can be conservatively assumed to be 5.

3.2. Searches Among List of 44 Candidate Sources

In order to reduce the large number of effective trials associated with scanning the entire sky, we also performed a search for the most significant of 44 *a priori* selected source candidates. The sources in this list have been selected according to observations in γ -rays or astrophysical models predicting neutrino emission.

3.3. Stacking Searches

Several sources of the same type may emit fluxes that are individually below the discovery potential but detectable as a class when summed up using the stacking technique. Here we report on the different catalogs of sources that have similar spectral behavior based on γ -ray observations or astrophysical models predicting neutrino emission. For these searches, the signal PDF \mathcal{S}_i^j of Eq. 1 is modified to accommodate multiple sources (see Ref. (Abbasi *et al.* 2011)). A prior knowledge of the expected luminosities of these sources can be utilized to weight the contribution of each source in the total signal PDF to make the search optimal for that signal hypothesis. Alternatively, an equal-weighting can be applied if there is no preferred model. In the following section we summarize all the stacking searches performed with 4 years of data. Most of these searches are updates from the previous results using 3 years of data (Aartsen *et al.* 2013c).

Updated searches : These searches have been previously carried out on three years of data (Aartsen *et al.* 2013c) and are now updated to include data from the first year of operation of the completed 86-string detector.

6 Milagro TeV gamma-ray sources. The authors of the model that motivated the original analysis have hence updated the models to reflect the newer γ -ray observations (Gonzalez-Garcia *et al.* 2014). For this reason, in this search an equal weight is used for each source in the likelihood with the intention of keeping our sensitivity optimal for all possible signal hypothesis.

127 local starburst galaxies. Sources compiled in Table A.1 in Ref. (Becker *et al.* 2009).

5 nearby clusters of galaxies. This search tests four models assuming different CR spatial distribution within the source (Murase *et al.* 2008).

10 SNRs associated with molecular clouds. This search is now updated to include more sources in the southern sky owing to our increased sensitivity in the southern sky due to new back-

ground rejection techniques. From the exhaustive online catalog SNRCat (Ferrand & Safi-Harb 2012), we select sources with confirmed molecular clouds associations. In order to keep the most promising neutrino emitters within the catalog, only sources that have been observed in the TeV or are younger than 10,000 yrs (potentially in the Sedov Blast wave phase (Sedov 1946) of expansion) are considered. The catalog contains 4 SNRs associated with molecular clouds in the northern sky (Abdo *et al.* 2007, 2009a,b, 2010; Ackermann *et al.* 2013; Fiasson *et al.* 2009) that were previously considered in Ref. (Aartsen *et al.* 2013c), and 6 newly introduced sources from SNRCat in the southern sky. These 6 sources are Sgr A East, Kes 75, 3C391, RX J1713.7-3946, CTB 37A and 1FGL J1717.9-3729.

233 Galaxies with super-massive black holes. A sample of AGNs within the GZK (Greisen 1966) radius as cataloged by Ref. (Caramete & Biermann 2010) keeping only sources more massive than 5×10^8 solar masses.

New searches: These are new searches introduced with the inclusion of the first year of data from the completed 86-string detector.

10 Galactic Pulsar Wind Nebulae. Pulsar Wind Nebulae (PWN) are potential emitters of neutrinos (Bednarek 2003). We carry out a stacked search for neutrinos coming from known PWNs within the Galaxy. From the confirmed PWNs in SNRCat (Ferrand & Safi-Harb 2012), we look at sources that are younger than 10,000 years as only younger PWNs are efficient accelerators (Bednarek 2003). We leave out sources that are already considered by the search for SNRs associated with molecular clouds. These criteria are fulfilled by 3 sources in the northern sky, namely the Crab Nebula, DA 530, G054.1+00.3 and 7 sources in the southern sky including the Pencil Nebula, W33 and MSH 11-54. These sources are weighted in likelihood by the inverse of their median age as provided by SNRCat (Ferrand & Safi-Harb 2012) to account for the higher fluxes expected from the youngest PWNs (Bednarek 2003).

30 Galactic SNRs. Galactic SNRs (Ferrand & Safi-Harb 2012) which neither have confirmed molecular cloud associations nor are PWNs are considered in this stacking search. As in the searches for PWNs and SNRs with Molecular Cloud associations, a cut on the SNR age is applied and only those younger than 10,000 years are selected (Castro *et al.* 2011). This requirement is met by 30 sources in total where 20 are located in the southern sky and 10 in the north. The inverse of the median age as provided by SNRCat (Ferrand & Safi-Harb 2012) is used as the weight for each source in likelihood in order to account for the fact that we expect the highest fluxes to come from the youngest SNRs. Remnants of recent prominent Supernovae such as Cassiopeia A and Tycho are considered within this search.

Blazars catalogs Three Blazar catalogs were composed from the Fermi LAT Second AGN Catalog (Ackermann *et al.* 2011) to allow for optimized analyses of the corresponding object classes. The first catalog contains Flat Spectrum Radio Quasars (FSRQ) which as suggested

by their broad line regions are thought to provide efficient photomeson production (Atoyan & Dermer 2001) in dense soft photon targets. The second set is formed by low-frequency peaked (LSP) BL Lac objects that are predicted to show a significant contribution from pion decays to the overall gamma-emission in the Synchrotron Proton Blazar Model (Mücke *et al.* 2003). Finally, p-p interaction models are covered by a catalog of the BL Lac objects with particularly hard gamma spectra and correspondingly large effective areas for neutrinos in IceCube (Neronov & Ribordy 2009).

The source selection and weighting for the FSRQ and LSP BL Lac catalogs, assuming prevalence of photo-hadronic neutrino production is based on the Fermi LAT gamma-flux. This motivates a weighting that is based on the measured gamma-fluxes but assumes the same spectral index for all sources (hereby denoted by W1).

In proton-proton interaction models, the energy spectrum of the produced neutral secondaries follows the initial cosmic ray spectrum down to a threshold below 1 GeV. The observation of the gamma-spectrum thus allows for a direct prediction of the proton spectrum behavior in the TeV range, which can be extrapolated to PeV energies to estimate the neutrino spectrum. Such an approach is not as easily possible for proton-gamma interaction models, as these typically have a lower energy threshold above TeV energies so that the photon (and neutrino) spectrum below the threshold does not allow for the derivation of the proton spectrum (Neronov & Ribordy 2009). Hence, the third catalog of hard γ -spectrum BL Lac objects motivates a selection and weighting based on the number of detectable neutrinos derived from the spectral shape measured by Fermi LAT (hereby denoted by W2).

Due to the variety of Blazar models and the large model uncertainties, both weighting schemes are applied to all three catalogs. Sources with negligible weights in both weighting schemes are discarded, resulting in 33 FSRQs, 27 LSP BL Lac objects and 37 hard γ -spectrum BL Lac objects.

This stacked search for blazars uses a reprocessed data set of the 79 string configuration that incorporates the new reconstruction methods presented in this work for IC-86, which were not yet available at the time of the previous analyses.

4. Results and Implications

In this section we summarize all the results from the different searches and their implication on astrophysical models of neutrino emission. While no significant excess has been found in any of the searches and all results are consistent with the background-only hypothesis, this has allowed us to set upper limits that exclude some of the models.

4.1. All-Sky Searches

4.1.1. All-Sky Point Source Scan

Figure 5 shows the result of the all-sky scan for point sources in terms of significance at each location in the sky given in equatorial coordinates. The most significant deviation in the northern sky has a pre-trial p-value of 4.81×10^{-6} , and is located at 29.25° r.a. and 10.55° dec. At this location, the best fit values of the number of source events, \hat{n}_s , and signal spectral index, $\hat{\gamma}$, are 43.0 and 2.88, respectively. In the southern sky, the most significant deviation has a pre-trial p-value of 6.81×10^{-6} and is located at 347.95° r.a. and -57.75° dec. Here, the best fit values of \hat{n}_s and $\hat{\gamma}$ are 13.0 and 3.95, respectively. After accounting for the trial factor associated with scanning the sky for the most significant spots, the post-trial p-values are 0.23 for the spot located in the northern sky and 0.44 for the spot located in the southern sky.

4.1.2. All-Sky Scans for Extended Sources

Table 2 summarizes the most significant hotspots in the sky from the scans for sources of various extensions. All observations were compatible with the background hypothesis. Figures 6 to 10 show the corresponding skymaps for 1° , 2° , 3° , 4° and 5° extension respectively.

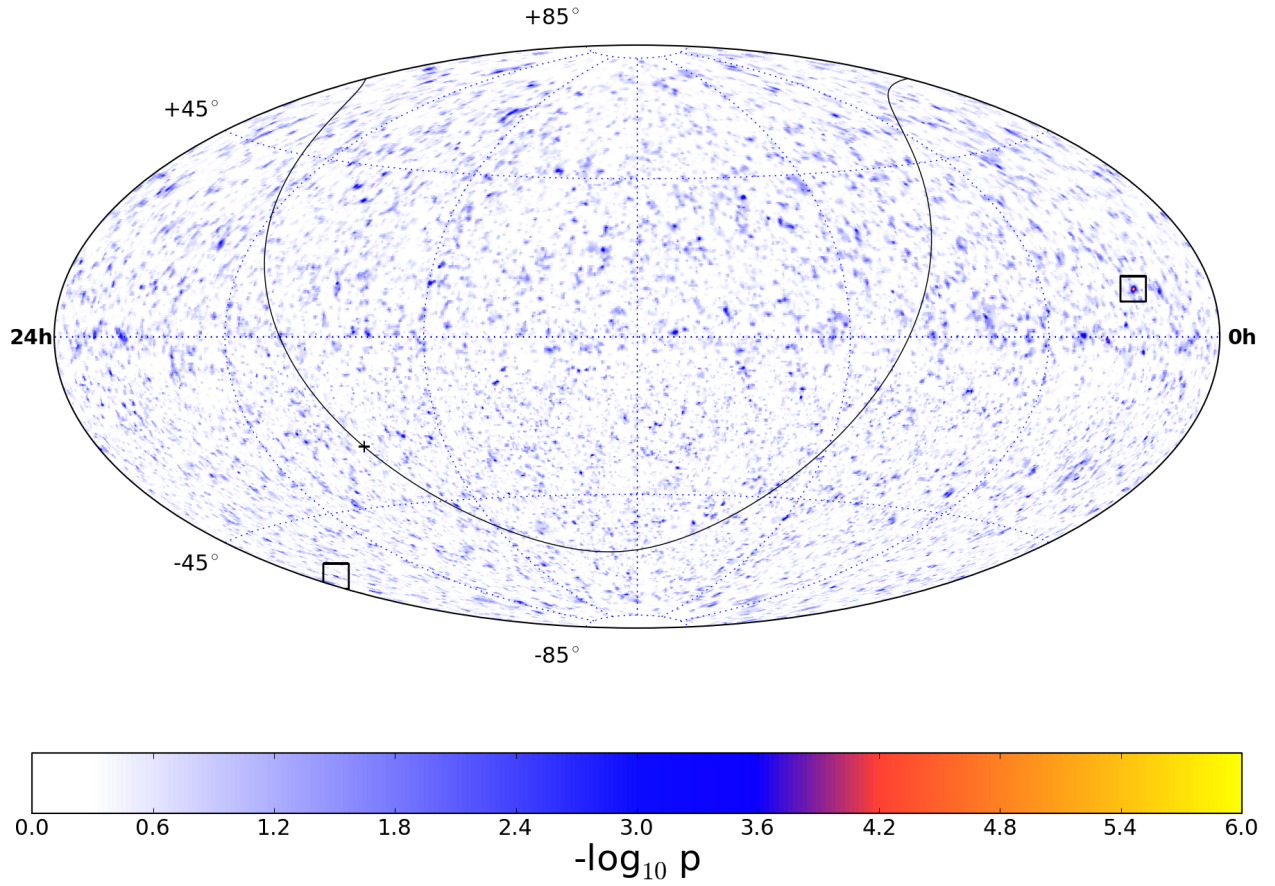


Fig. 5.— Pre-trial significance skymap in equatorial coordinates (J2000) of the all-sky point source scan for the combined four year data sample. The black line indicates the Galactic plane, and the black plus sign indicates the Galactic Center. The most significant fluctuation in each hemisphere is indicated with a square marker.

Extension [°]	r.a. [°]	dec. [°]	\hat{n}_S	$\hat{\gamma}$	p-value (pre-trial)	p-value (post-trial)
1°	286.25	-43.25	49.6	2.65	6.75×10^{-5}	0.58
2°	248.75	62.75	58.2	2.38	5.52×10^{-4}	0.87
3°	30.75	-30.25	93.6	3.10	1.22×10^{-3}	0.81
4°	30.75	-30.25	99	3.10	3.29×10^{-3}	0.81
5°	251.75	61.25	102	2.54	1.06×10^{-2}	0.91

Table 2:: Summary of the results from the extended all-sky survey. The coordinates of the most significant spots located for each source extension hypothesis are given together with the respective p -values.

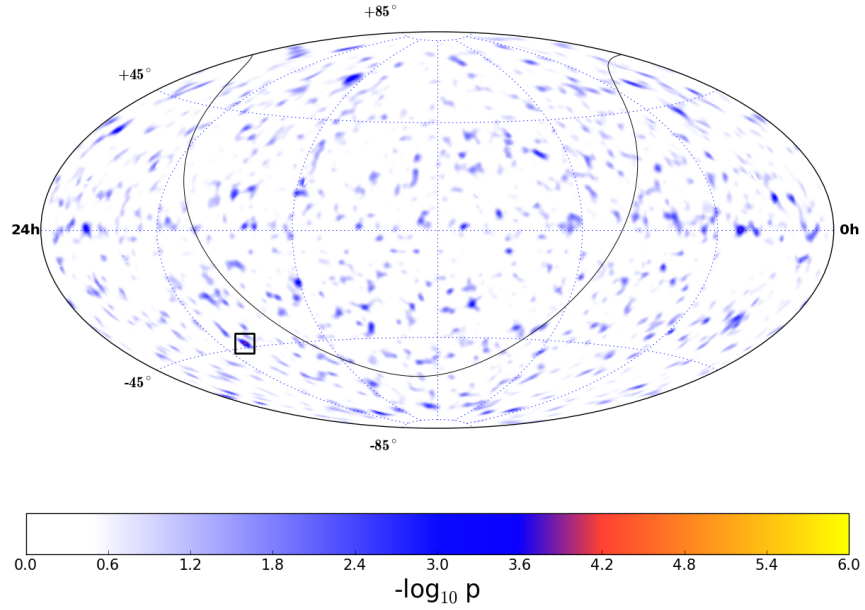


Fig. 6.— Pre-trial significance skymap from the all-sky scan for sources of 1° extension in equatorial coordinates. The black line indicates the Galactic Plane. The most significant fluctuation is indicated with a square marker.

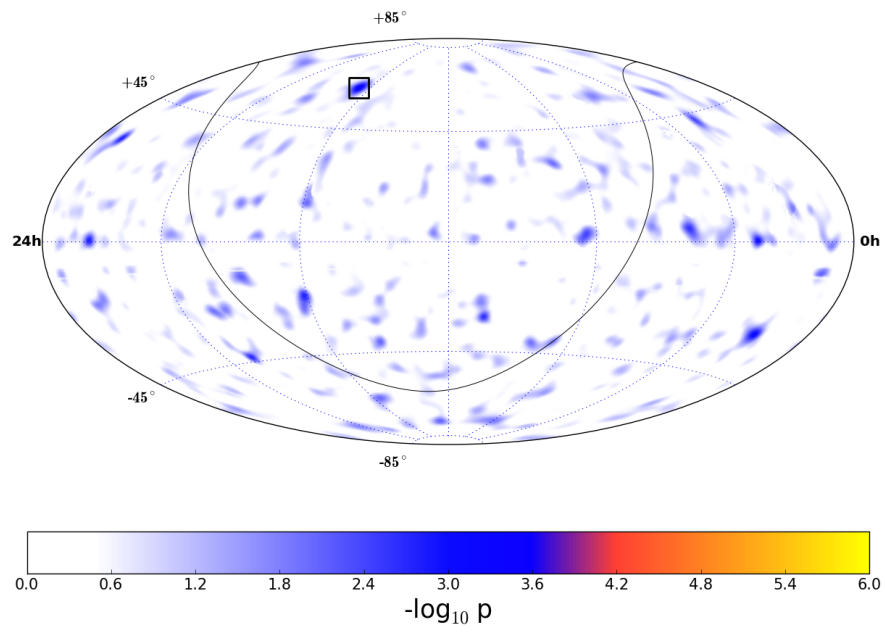


Fig. 7.— Same as Fig. 6 but for sources of 2° extension.

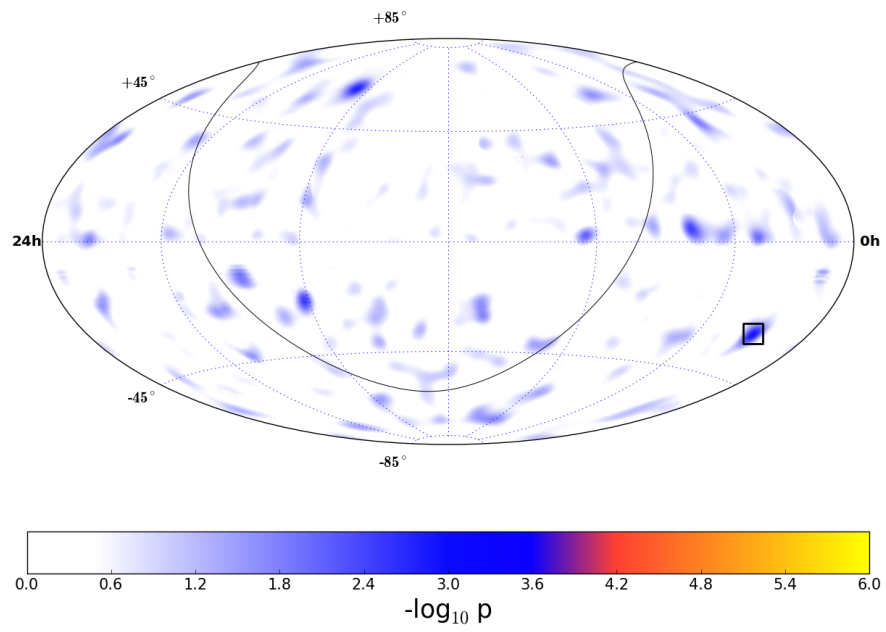


Fig. 8.— Same as Fig. 6 but for sources of 3° extension.

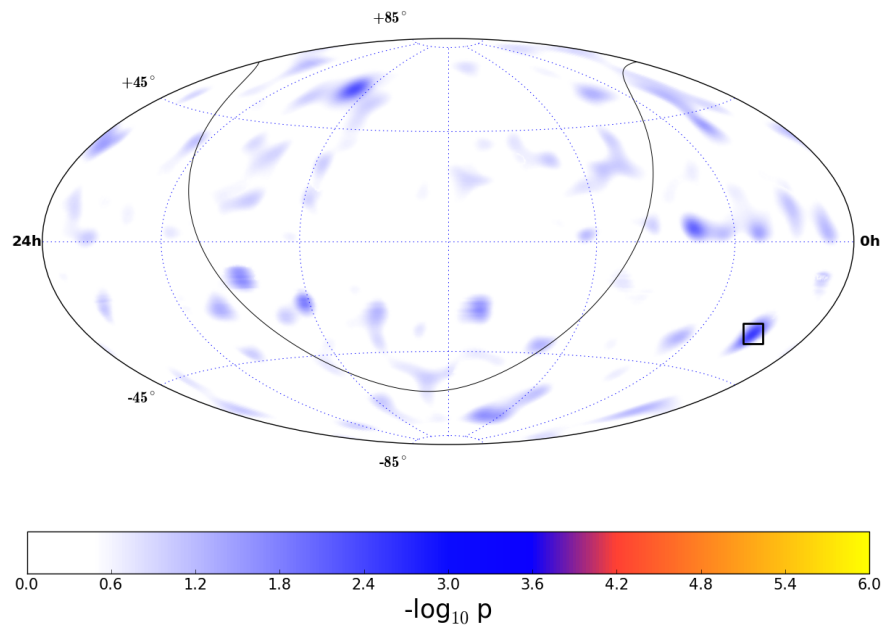


Fig. 9.— Same as Fig. 6 but for sources of 4° extension.

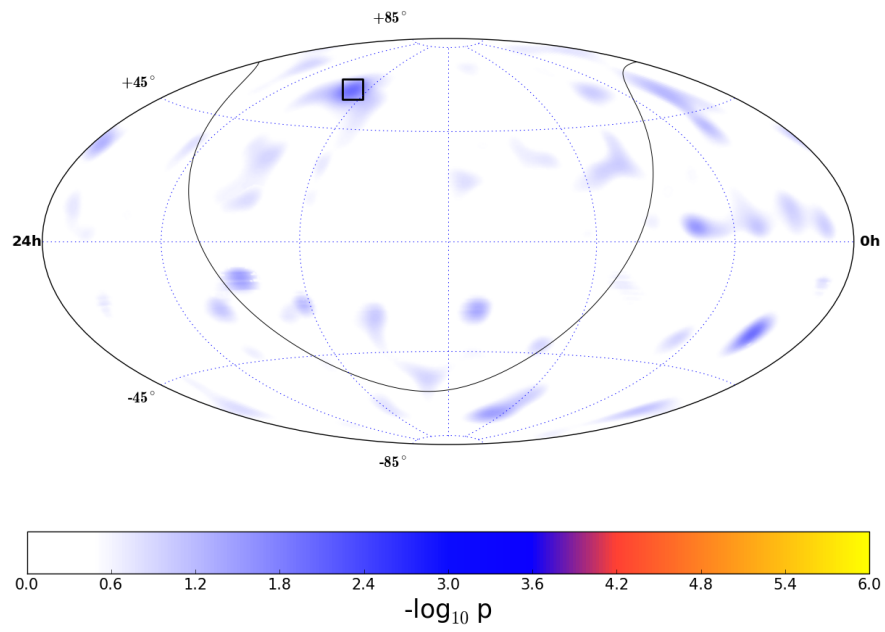


Fig. 10.— Same as Fig. 6 but for sources of 5° extension.

Since filtering streams, reconstructions and detector configurations evolved with time, we also examined each of the four years of data independently as an a posteriori cross-check. The largest fluctuation was observed for the one degree extension hypothesis in data from the 79 string configuration at 266.75 r.a. and 13.25 dec, where 0.35% of scrambled maps in that year resulted in a fluctuation more significant than the one observed. Since we scanned over 5 different extensions for every year, the corresponding trial-corrected p-value is 7.2%, well compatible with a background fluctuation. The hot-spot seems to be driven by a single well-reconstructed very high-energy event which, when folded with the wider source template, overlaps with some nearby lower energy ones. From calibration using the shadow of the moon (Aartsen *et al.* 2013e), there is no evidence for a systematic error in IceCube’s point spread function that could lead to the observed spread for events originating from a point-like source. The region is not significant in any of the other years of data.

4.2. List of 44 Candidate Sources

The search for neutrino emission from an *a priori* list of 44 candidate sources produced the results shown in Tables 3 and 4. In the northern sky, 1ES 0229+200 has the strongest upward fluctuation. The pre-trial p-value of such a fluctuation is 0.053, but after considering the random chance of observing a fluctuation as strong or stronger than this in any of the sources, the post-trial p-value is 0.61. In the southern sky, PKS 0537-441 has the strongest upward fluctuation, with a pre-trials p-value of 0.083 and a post-trials p-value of 0.33. Upper limits on the E^{-2} muon neutrino flux for 90% confidence level (C.L.) from each source are listed in the table, and are shown along with the analysis sensitivity in Figure 11.

While many baseline models for CR acceleration and high-energy neutrino production predict E^{-2} neutrino spectra, individual sources with unique conditions can produce significantly different spectra. Models for any source in the sky can be tested with the analysis method used in this work, and a number of individual sources were previously considered in Ref. (Aartsen *et al.* 2013c). Here, we update the 90% C.L. upper limits on three models of neutrino emission from the Crab Nebula (Fig. 12) as well as three Galactic supernova remnants (Fig. 13).

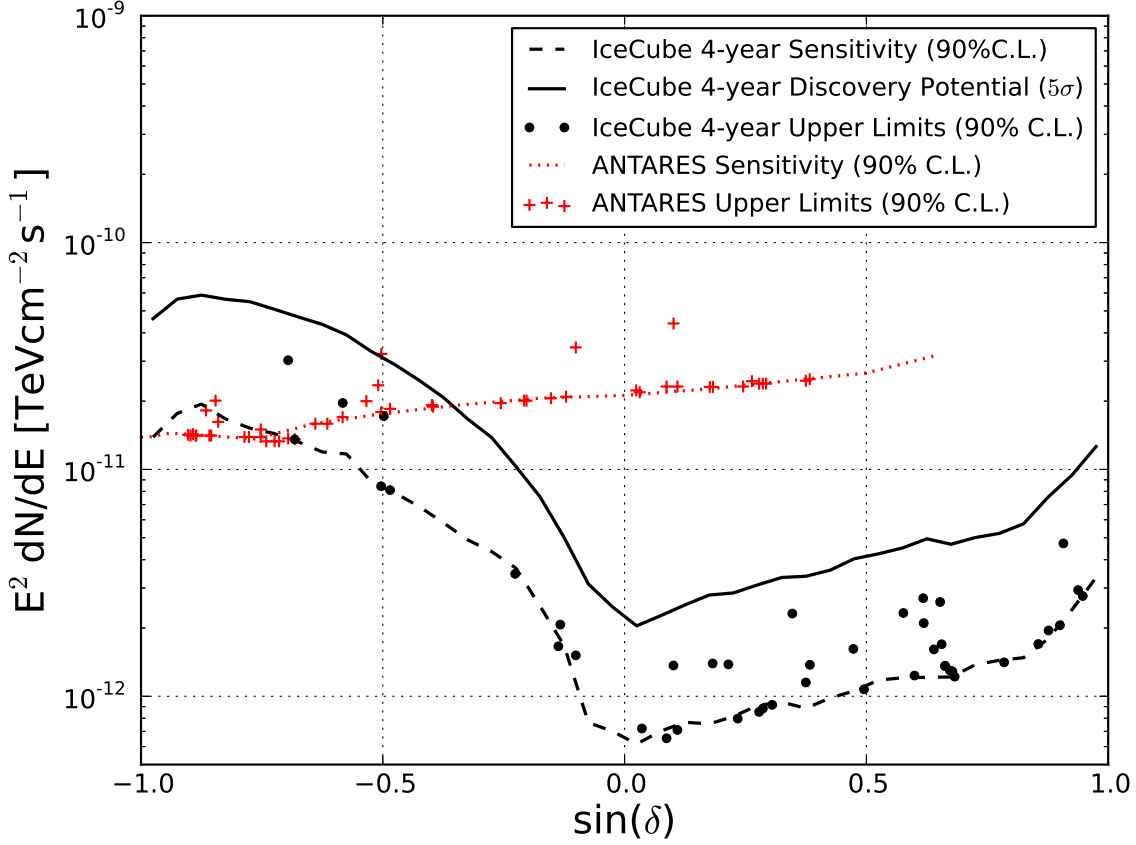


Fig. 11.— Muon neutrino upper limits with 90% C.L. evaluated for the 44 sources (dots), for the combined four years of data (40, 59, 79, and 86 string detector configurations). The solid black line is the flux required for 5σ discovery of a point source emitting an E^{-2} flux at different declinations while the dashed line is the median upper limit or sensitivity also for a 90% C.L. The ANTARES sensitivities and upper limits are also shown (Adrián-Martínez *et al.* 2014). For sources in the southern hemisphere, ANTARES constrains neutrino fluxes at lower energies than this work.

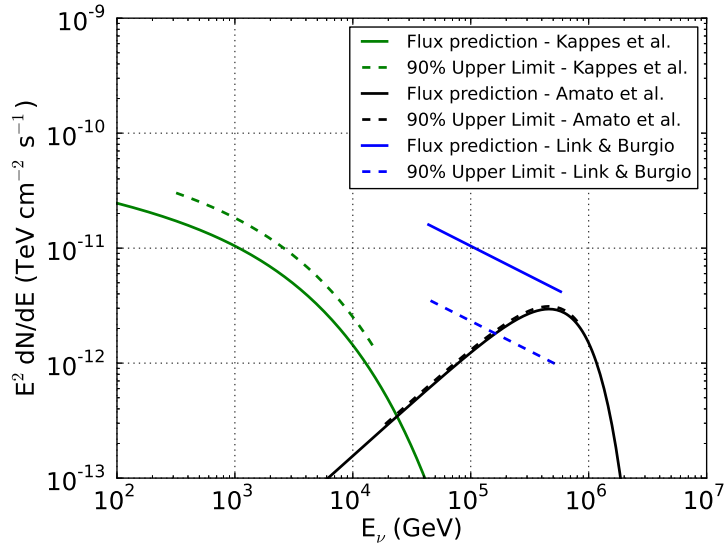


Fig. 12.— Flux predictions (solid) for three models of neutrino emission from the Crab Nebula, with their associated 90% C.L. upper limits (dashed) for an energy range containing 90% of the signal. Both the model from Amato *et al.* (Amato *et al.* 2003) and the most optimistic model from Link & Burgio (Link & Burgio 2005, 2006) are now excluded at 90% confidence level. For the gamma-ray based model from Kappes *et al.* (Kappes *et al.* 2007), the upper limit is still a factor of 1.75 above the prediction.

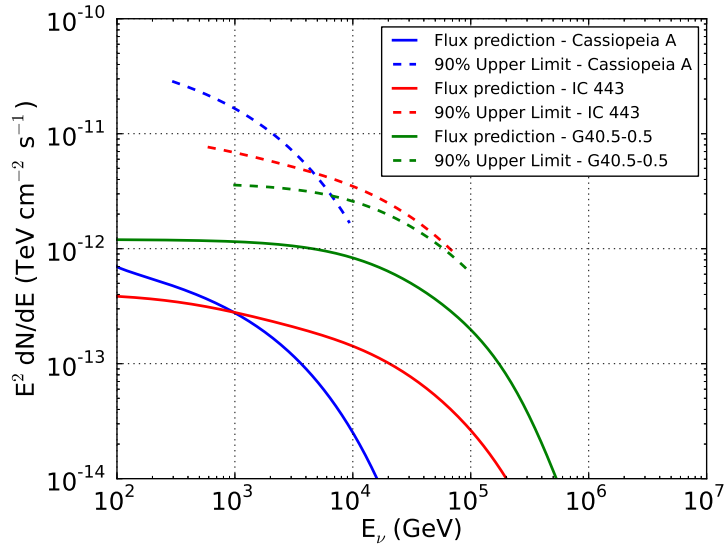


Fig. 13.— Flux predictions (solid) and upper limits (dashed) for three Galactic supernova remnants. The neutrino models, based of fitted gamma-ray observations, are from (Mandelartz & Tjus 2013). For the source with the highest predicted flux, G40.5-0.5, the upper limit is a factor of three above the model.

Table 3:: Results for Galactic objects on the *a priori* search list.

Category	Source	r.a. [°]	dec. [°]	p-value	\hat{n}_S	$\hat{\gamma}$	B_{1°	$\Phi_{\nu_\mu + \bar{\nu}_\mu}^{90\%}$
SNR	TYCHO	6.36	64.18	–	0.0	–	17.8	2.06
	Cas A	350.85	58.81	–	0.0	–	17.8	1.70
	IC443	94.18	22.53	0.35	4.6	3.9	27.8	1.38
HMXB /mqso	LSI +63 303	40.13	61.23	–	0.0	–	17.8	1.95
	Cyg X-3	308.11	40.96	0.42	3.7	3.9	21.5	1.70
	Cyg X-1	299.59	35.20	0.18	8.9	3.9	23.4	2.33
	HESS J0632+057	98.25	5.80	0.14	13.4	3.4	37.0	1.37
	SS433	287.96	4.98	–	0.0	–	37.6	0.65
Star For- mation Region	Cyg OB2	308.08	41.51	–	0.0	–	21.0	1.36
pulsar/ PWN	MGRO J2019+37	305.22	36.83	–	0.0	–	23.1	1.23
	Crab Nebula	83.63	22.01	0.44	4.4	3.9	27.8	1.15
	Geminga	98.48	17.77	–	0.0	–	30.7	0.92
Galactic Center	Sgr A*	266.42	-29.01	–	0.0	–	36.6	8.11

Continued on next page

Table 3 – *Continued from previous page*

Category	Source	r.a. [°]	dec. [°]	p-value	\hat{n}_S	$\hat{\gamma}$	B_{1°	$\Phi_{\nu_\mu + \bar{\nu}_\mu}^{90\%}$
Not identified	MGRO J1908+06	286.98	6.27	–	0.0	–	36.4	0.71

Note. – Sources are grouped according to their classification as High-Mass X-ray binaries or micro-quasars (HMXB/mqso), SNRs, Pulsar Wind Nebulas (PWNs), star formation regions and unidentified sources. The p-value is the pre-trial probability of compatibility with the background-only hypothesis. The \hat{n}_S and $\hat{\gamma}$ columns give the best-fit number of signal events and spectral index of a power-law spectrum. When $\hat{n}_S = 0$, no p-value or $\hat{\gamma}$ are reported. The eighth column gives the number of background events in a circle of 1° around the search coordinates. The last column shows the upper limits based on the classical approach (Neyman 1937) for an E^{-2} flux normalization of $\nu_\mu + \bar{\nu}_\mu$ flux in units of $10^{-12} \text{ TeV}^{-1} \text{ cm}^{-2} \text{ s}^{-1}$.

Table 4:: Results for extragalactic objects on the *a priori* search list.

Category	Source	r.a. [°]	dec. [°]	p-value	\hat{n}_S	$\hat{\gamma}$	B_{1°	$\Phi_{\nu_\mu + \bar{\nu}_\mu}^{90\%}$
BL Lac	S5 0716+71	110.47	71.34	–	0.0	–	16.5	2.77
	1ES 1959+650	300.00	65.15	0.083	9.8	3.2	17.7	4.72
	1ES 2344+514	356.77	51.70	–	0.0	–	19.1	1.41
	3C66A	35.67	43.04	–	0.0	–	20.5	1.220
	H 1426+428	217.14	42.67	–	0.0	–	20.8	1.29
	BL Lac	330.68	42.28	–	0.0	–	20.8	1.30
	Mrk 501	253.47	39.76	0.45	3.2	3.7	22.1	1.61
	Mrk 421	166.11	38.21	0.26	3.8	1.9	22.4	2.10
	W Comae	185.38	28.23	0.34	1.4	1.6	25.9	1.62
	1ES 0229+200	38.20	20.29	0.053 ^a	16.0	3.7	28.6	2.32
	PKS 0235+164	39.66	16.62	–	0.0	–	31.4	0.88
	PKS 2155-304	329.72	-30.23	–	0.0	–	37.0	8.43
PKS 0537-441	84.71	-44.09	0.083 ^b	6.3	3.9	35.2	30.03	
FSRQ	4C 38.41	248.81	38.13	0.12	10.6	2.8	22.4	2.71
	3C 454.3	343.49	16.15	–	0.0	–	31.4	0.85
	PKS 0528+134	82.73	13.53	–	0.0	–	32.3	0.80
	PKS 1502+106	226.10	10.49	0.21	6.1	2.3	33.2	1.39

Continued on next page

Table 4 – *Continued from previous page*

Category	Source	r.a. [°]	dec. [°]	p-value	\hat{n}_S	$\hat{\gamma}$	B_{1°	$\Phi_{\nu_\mu + \bar{\nu}_\mu}^{90\%}$
	3C 273	187.28	2.05	0.45	3.2	2.6	38.9	0.72
	3C279	194.05	-5.79	–	0.0	–	33.5	1.51
	QSO 2022-077	306.42	-7.64	0.45	1.3	2.0	34.1	2.07
	PKS 1406-076	212.24	-7.87	–	0.0	–	34.1	1.66
	QSO 1730-130	263.26	-13.08	–	0.0	–	37.1	3.46
	PKS 1622-297	246.53	-29.86	0.13	6.2	2.7	36.6	17.17
	PKS 1454-354	224.36	-35.65	0.2	5.4	3.9	35.6	19.64
Starburst	M82	148.97	69.68	–	0.0	–	16.3	2.94
Radio	NGC 1275	49.95	41.51	–	0.0	–	21.0	1.36
Galaxies	Cyg A	299.87	40.73	0.18	1.8	1.5	21.5	2.60
	3C 123.0	69.27	29.67	–	0.0	–	25.7	1.07
	M87	187.71	12.39	0.26	8.8	3.9	32.4	1.38
	Cen A	201.37	-43.02	–	0.0	–	35.5	13.57

Note. – Sources are grouped according to their classification as BL Lac objects, Radio Galaxies, Flat-Spectrum Radio Quasars (FSRQ) and Starburst galaxies. The p-value is the pre-trial probability of compatibility with the background-only hypothesis. The \hat{n}_S and $\hat{\gamma}$ columns give the best-fit number of signal events and spectral index of a power-law spectrum. When $\hat{n}_S = 0$, no p-value or $\hat{\gamma}$ are reported. The eighth column gives the number of background events in a circle of 1° around the search coordinates. The last column shows the upper limits based on the classical approach (Neyman 1937) for an E^{-2} flux normalization of $\nu_\mu + \bar{\nu}_\mu$ flux in units of $10^{-12} \text{ TeV}^{-1} \text{ cm}^{-2} \text{ s}^{-1}$.

^{a,b}Most significant p-value in the northern and southern skies, respectively, among all Galactic and extragalactic objects on the *a priori* search list.

4.3. Stacking Searches

The results of all stacking searches are compatible with the background only hypothesis and are summarized in Table 5. The most significant deviation from the background only hypothesis was observed in the stacked search for neutrino emission from the six Milagro TeV Gamma ray sources, with a p-value of 0.02. The fitted spectral index of 3.95 however suggests that only low energy events contribute towards the observation and the observed significance is from spatial clustering

only. While Ref. (Halzen *et al.* 2008) predicts a flux of much higher energy neutrinos from these sources, the assumptions made about the gamma ray spectra of the sources in Ref. (Halzen *et al.* 2008) have later proved to be too optimistic (Abdo *et al.* 2012). Subsequently, the authors have updated the models (Gonzalez-Garcia *et al.* 2014). Fig 14 shows the IceCube upper limits to the model of Ref. (Halzen *et al.* 2008). In Fig 14, we also compare limits on neutrino fluxes from galaxy clusters to the model from Ref. (Murase *et al.* 2008).

Catalog		\hat{n}_S	$\hat{\gamma}$	p-value	$\Phi_{\nu_\mu+\bar{\nu}_\mu}^{90\%}$
Milagro 6		51.4	3.95	0.02	$1.98 \times \text{M.F.}$ (Halzen <i>et al.</i> 2008)
Galaxy Clusters	<i>Model A</i>	1.4	3.95	0.50	$3.89 \times \text{M.F.}$ (Murase <i>et al.</i> 2008)
	<i>Model B</i>	12.6	3.95	0.48	$6.17 \times \text{M.F.}$ (Murase <i>et al.</i> 2008)
	<i>Central AGN</i>	0.0	–	–	$1.54 \times \text{M.F.}$ (Murase <i>et al.</i> 2008)
	<i>Isobaric</i>	0.0	–	–	$4.65 \times \text{M.F.}$ (Murase <i>et al.</i> 2008)
Starburst Galaxies		0.0	–	–	$7.93 \times 10^{-12} \times \text{E}^{2.0}$
MC Associated SNRs		0.0	–	–	$1.60 \times 10^{-9} \times \text{E}^{2.7}$
Supermassive Black Holes		17.1	3.95	0.43	$6.88 \times 10^{-12} \times \text{E}^{2.0}$
Young SNRs		0.0	–	–	$4.83 \times 10^{-12} \times \text{E}^{2.0}$
Young PWNs		0.0	–	–	$3.12 \times 10^{-12} \times \text{E}^{2.0}$
FSRQs	W1	9.8	2.45	0.31	$3.46 \times 10^{-12} \times \text{E}^{2.0}$
	W2	15.4	2.75	0.19	$34.3 \times \text{M.F.}$
LSP BL Lacs	W1	11.9	3.25	0.38	$5.24 \times 10^{-12} \times \text{E}^{2.0}$
	W2	21.8	3.59	0.10	$13.5 \times \text{M.F.}$
Hard BL Lacs	W1	0	–	–	$3.73 \times 10^{-12} \times \text{E}^{2.0}$
	W2	17.5	3.95	0.29	$0.284 \times \text{M.F.}$

Table 5:: Results of the stacked searches for emission from source catalogs. M.F. stands for the model flux as described in the references motivating the analyses. $\Phi_{\nu_\mu+\bar{\nu}_\mu}^{90\%}$ is the 90% Confidence Level upper limit on the combined flux of ν_μ and $\bar{\nu}_\mu$ from the catalogs. The $\text{E}^{2.0}$ limits are in units of $\text{TeV}^1 \text{cm}^{-2} \text{s}^{-1}$.

4.4. Systematic Uncertainties

In all analyses described here the background is estimated by scrambling the detector data in right ascension and is independent of theoretical uncertainties on fluxes of atmospheric neutrino and muons as well as uncertainties in the simulation of the detector. The p-values are therefore robust against most sources of systematic error. Upper limits and analysis sensitivities however are calculated by simulating the detector response to neutrinos. Detector uncertainties including the optical properties of the ice and the absolute efficiency of the optical modules can affect the reported sensitivities and upper limits.

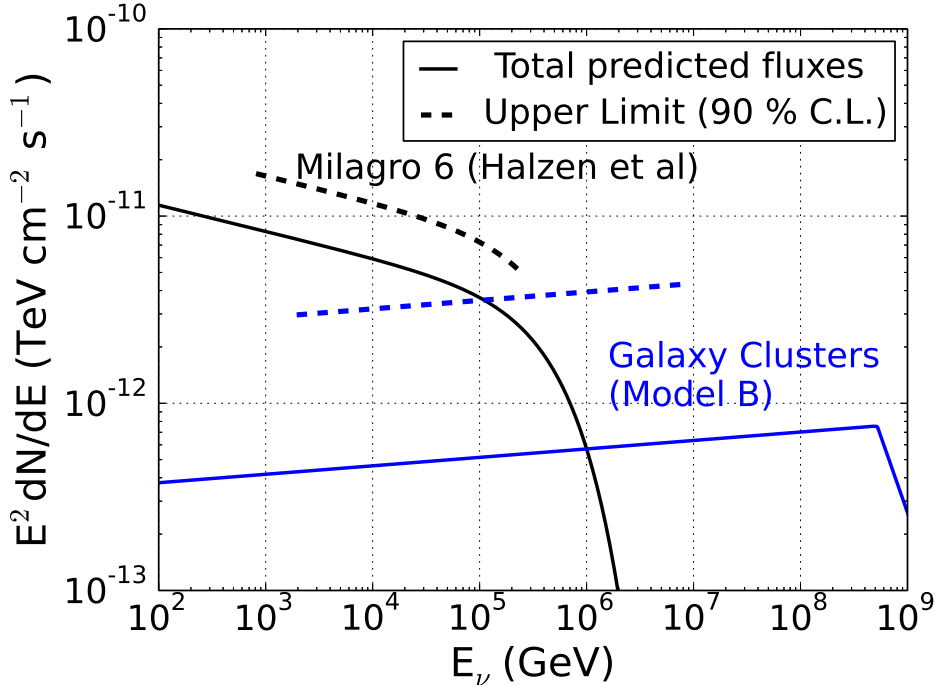


Fig. 14.— IceCube 90% C.L. upper limits to the models of (Halzen *et al.* 2008) and (Murase *et al.* 2008).

After a detailed discussion of all relevant systematic uncertainties, Ref. (Aartsen *et al.* 2013c) concludes that the level of uncertainty in the analysis using three years of data is about 18%. Since 65% of the data used here is the same as in Ref. (Aartsen *et al.* 2013c) and the techniques for the new event selection and analyses are similar, the systematic uncertainty on the 4 year sample is about the same. However, the added year of data utilizes a new muon track reconstruction, which is more sensitive to uncertainties in the optical properties of the ice. We re-evaluate the effect of the ice properties on the analysis for the 2011-2012 data, finding a corresponding systematic uncertainty of +16%/-8%. This is incorporated into the overall systematic uncertainty by averaging it with the ice model effect from the previous years. The resulting overall systematic uncertainty on the quoted sensitivities and upper limits is 21%.

5. Conclusions

No evidence of neutrino emission from point-like or extended sources was found in four years of IceCube data. Searches for emissions from point-like and extended sources anywhere in the sky, from a pre-defined candidate source list and from stacked source catalogs all returned results

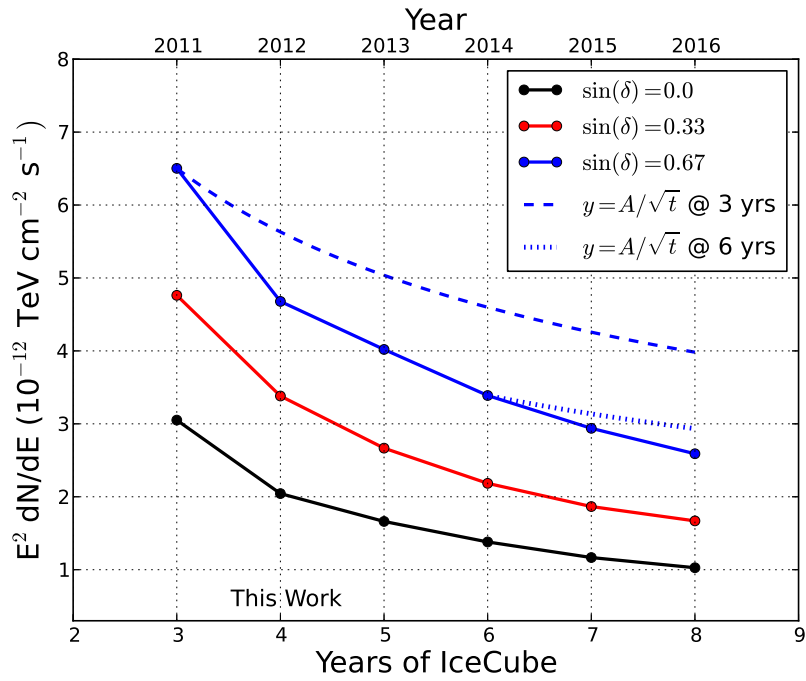


Fig. 15.— Predicted E^{-2} discovery potential as a function of years of running time of the IceCube Observatory for three different declinations (solid lines). Due to the relatively low background rate in this analysis, the discovery potential will continue to improve faster than the square-root of time limit (dashed, dotted lines).

consistent with the background-only hypothesis. 90% C.L. upper limits on the muon neutrino fluxes for models from a variety of sources were calculated and compared to predictions. The most optimistic models considered here can be excluded at 90% C.L. and in other cases limits are a factor of two to four above the predictions. This analysis includes data from the completed IceCube array, taken between May 2011 and May 2012. IceCube will continue to run in this configuration for the foreseeable future. Future analyses will benefit from this improved integration time and the evolution of the analysis sensitivity as a function of years of data-taking is shown in Figure 15. Within a few years the analyses will surpass the sensitivity necessary to test a wider variety of neutrino point source models. Future developments in background rejection techniques and reconstruction algorithms may lead to improvements faster than predicted in Figure 15.

Acknowledgements

We acknowledge the support from the following agencies: U.S. National Science Foundation-Office of Polar Programs, U.S. National Science Foundation-Physics Division, University of Wisconsin Alumni Research Foundation, the Grid Laboratory Of Wisconsin (GLOW) grid infrastructure at the University of Wisconsin - Madison, the Open Science Grid (OSG) grid infrastructure; U.S. Department of Energy, and National Energy Research Scientific Computing Center, the Louisiana Optical Network Initiative (LONI) grid computing resources; Natural Sciences and Engineering Research Council of Canada, WestGrid and Compute/Calcul Canada; Swedish Research Council, Swedish Polar Research Secretariat, Swedish National Infrastructure for Computing (SNIC), and Knut and Alice Wallenberg Foundation, Sweden; German Ministry for Education and Research (BMBF), Deutsche Forschungsgemeinschaft (DFG), Helmholtz Alliance for Astroparticle Physics (HAP), Research Department of Plasmas with Complex Interactions (Bochum), Germany; Fund for Scientific Research (FNRS-FWO), FWO Odysseus programme, Flanders Institute to encourage scientific and technological research in industry (IWT), Belgian Federal Science Policy Office (Belspo); University of Oxford, United Kingdom; Marsden Fund, New Zealand; Australian Research Council; Japan Society for Promotion of Science (JSPS); the Swiss National Science Foundation (SNSF), Switzerland; National Research Foundation of Korea (NRF); Danish National Research Foundation, Denmark (DNRF)

REFERENCES

- M. G. Aartsen *et al.* [IceCube Coll.] Nucl. Instr. Meth. **A711** (2013) 73.
- M. G. Aartsen *et al.* [IceCube Coll.] Nucl. Instr. Meth. **A736** (2013) 143.
- M. G. Aartsen *et al.* [IceCube Coll.] ApJ **779** (2013) 132.
- M. G. Aartsen *et al.* [IceCube Coll.] Science **342** (2013) 947.

- M. G. Aartsen *et al.* [IceCube Coll.] (2013) arXiv:1305.6811.
- M. G. Aartsen *et al.* [IceCube Coll.] JINST **9** (2014) P03009.
- M. G. Aartsen *et al.* [IceCube Coll.] (2014) arXiv 1405.5303.
- R. Abbasi *et al.* [IceCube Coll.] Nucl. Instr. Meth. **A601** (2009) 294.
- R. Abbasi *et al.* [IceCube Coll.] Nucl. Instr. Meth. **A618** (2010) 139.
- R. Abbasi *et al.* [IceCube Coll.], ApJ **732** (2011) 18.
- A. A. Abdo *et al.*, ApJ **664** (2007) L91.
- A. A. Abdo *et al.* [Fermi Coll.], ApJ **706** (2009) L1.
- A. A. Abdo *et al.* [Milagro Coll.], ApJ. **700** (2009) L127.
- A. A. Abdo *et al.* [Fermi Coll.], Science **327** (2010) 1103.
- A. A. Abdo *et al.*, ApJ **753** (2012) 159.
- A. Achterberg *et al.*, [IceCube Coll.] Astropart. Phys. **26** (2006) 155.
- M. Ackermann *et al.*, ApJ **743** (2011) 171.
- M. Ackermann *et al.* [Fermi Coll.], Science **339** (2013) 807.
- S. Adrián-Martínez *et al.* [Antares Coll.] ApJ **786** (2014) L5.
- J. Ahrens *et al.* Nucl. Instrum. Meth. **A524** (2004) 169.
- J. Alvarez-Muñiz and F. Halzen, ApJ **576** (2002) L33.
- E. Amato, D. Guetta and P. Blasi, Astron. Astrophys. **402** (2003) 827.
- L. Anchordoqui and T. Montaruli, Ann. Rev. Nucl. Part. Sci. **60** (2010) 129.
- L. Anchordoqui *et al.* JHEAp. **1** (2014) 1.
- A. Atoyan & C.D. Dermer, Phys. Rev. Lett. **87** (2001) 221102.
- J. Becker, Phys. Rep. **458** (2008) 173.
- J. Becker *et al.*, (2009) arXiv:0901.1775.
- W. Bednarek, Astron. Astrophys. **407** (2003) 1.
- J. Braun *et al.*, Astropart. Phys. **33** (2010) 175.
- L. Caramete & P.L. Biermann, Astron. Astrophys. **521** (2010) A55.

- S. Carrigan *et al.* [HESS Coll.] (2013) arXiv:1307.4868v2.
- D. Castro *et al.*, ApJ **734** (2011) 85.
- V. Cavasinni *et al.*, Astropart. Phys. **26** (2006) 41.
- D. De Marco, P. Blasi, P. Hansen, and T. Stanev. Phys. Rev. **D73** (2006) 043004.
- W. Essey, O. E. Kalashev, A. Kusenko, and J. F. Beacom, Phys. Rev. Lett. **104** (2010) 141102.
- G. Ferrand and S. Safi-Harb, Advances in Space Research **49** (2012) 1313.
- A. Fiasson *et al.* [HESS Coll.], in *Proc. of the 31st Int. Cosmic Ray Conf.*, Lodz, Poland (2009).
- M. C. Gonzalez-Garcia *et al.* Astrop. Phys. **57** (2014) 39.
- K. Greisen, Phys. Rev. Lett. **16** (1966) 748.
- D. Guetta *et al.* Astrop. Phys. **20** (2004) 429.
- F. Halzen and D. Hooper, Rep. Progr. Phys. **65** (2002) 1025.
- F. Halzen, A. Kappes and A. O’Murchadha, Phys. Rev. **D78** (2008) 063004.
- M. Honda *et al.*, Phys.Rev. **D75** (2007) 043006.
- O. E. Kalashev, A. Kusenko, and W. Essey, Phys. Rev. Lett. **111** (2013) 041103.
- A. Kappes *et al.*, ApJ **656** (2007) 870.
- M. D. Kistler & J. F. Beacom, Phys. Rev. **D74** (2006) 0607082.
- B. C. Lacki *et al.*, ApJ **734** (2011) 107.
- J. G. Learned and K. Mannheim, Ann. Rev. Nucl. Part. Sci. **50** (2000) 679.
- B. Link & F. Burgio, Phys. Rev. Lett. **94** (2005) 181101.
- B. Link & F. Burgio, Mon. Not. Roy. Astron. Soc. **371** (2006) 375.
- A. Loeb and E. Waxman, JCAP **0605** (2006) 003.
- M. Mandelartz & J. Becker Tjus, (2013) arxiv:1301.2437.
- P. Mészáros, Rep. Prog. Phys. **69** (2006) 2259.
- A. Mücke *et al.*, Astropart.Phys. **18** (2003) 593.
- K. Murase *et al.*, ApJ **689** (2008) L105.
- K. Murase and J. F. Beacom, JCAP **02** (2012) 028.

- K. Murase, M. Ahlers, and B. C. Lacki, Phys. Rev. **D88** (2013) 121301.
- K. Murase, Y. Inoue, and C. D. Dermer, (2014) arXiv:1403.4089.
- A. Neronov & M. Ribordy, Phys.Rev. **D80** (2009) 083008.
- T. Neunhöffer, Astropart. Phys. **26** (2006) 220.
- J. Neyman. Phil. Trans. Royal Soc. London A **236** (1937) 333.
- G. E. Romero and D. F. Torres, ApJ **586** (2003) L33.
- L. Sironi and A. Spitkovsky, ApJ **726** (2011) 75.
- L. I. Sedov, Journal of Applied Mathematics and Mechanics, Vol. **10** (1946) 241.
- F. W. Stecker, C. Done, M. H. Salamon, and P. Sommers, Phys. Rev. Lett. **66** (1991) 2697.
- C. Tchernin *et al.*, Astron. Astrophys. **560** (2013) A67.
- F. Vissani, F. Aharonian, and N. Sahakyan, Astrop. Phys. **34** (2011) 778.
- E. Waxman and J. Bahcall, Phys. Rev. Lett. **78** (1997) 2292.
- E. Waxman and J. Bahcall, Phys. Rev. **D59** (1999) 023002.
- N. Whitehorn, J. van Santen and S. Lafebre, CPC **184** (2013), 2214-2220.
- B. Wolfe, F. Melia, R. M. Crocker, and R. R. Volkas, ApJ **687** (2008) 193.